The replacement of a carbonate rock by fluorite: kinetics and microstructure

Elisabete Trindade Pedrosa, Lena Boeck, Christine V Putnis, Andrew Putnis

The replacement of a carbonate rock by fluorite: kinetics and microstructure

Elisabete Trindade Pedrosa[1], Lena Boeck[1], Christine V. Putnis[1,2], Andrew Putnis[1,3]

[1]Institut für Mineralogie, University of Münster, Corrensstrasse 24, 48149 Münster, Germany

[2]Department of Chemistry, Curtin University, 6845 Perth, Australia

[3]The Institute for Geoscience Research (TIGeR), Curtin University, 6845 Perth, Australia

Abstract

Understanding the mechanism and kinetics of the replacement of carbonates by fluorite has application in Earth sciences and engineering. Samples of Carrara marble were reacted with an ammonium fluoride (NH_4F) solution for different reaction times and temperatures. The microstructure of the product phase (fluorite) was analyzed using SEM. The kinetics of replacement was monitored using Rietveld analysis of X-ray powder diffraction patterns of the products. After reaction, all samples preserved their size and external morphology (a pseudomorphic replacement). The grain boundaries of the original marble were preserved although each calcite grain was replaced by multiple fine crystals of fluorite creating inter-crystal porosity. The empirical activation energy E_a (kJ/mol) of the replacement reaction was determined by both model-fitting and model-free methods. The isoconversional method yielded an empirical activation energy of 41 kJ/mol, and a statistical approach applied to the model-fitting method revealed that the replacement of Carrara marble by fluorite is better fitted to a diffusion-controlled process. These results suggest that the replacement reaction is dependent on the ion diffusion rate in the fluid phase through the newly formed porosity.

Keywords: Calcite, fluorite, replacement, dissolution-precipitation, kinetics, porosity

Introduction

Mineral replacement reactions may occur in any situation that involves the reequilibration between a solid and a fluid phase and are commonly controlled by an interface-coupled dissolution-precipitation mechanism (Putnis 2002, 2009; Putnis and Putnis 2007). Such reactions occur commonly in the crust of the Earth, where aqueous fluids are ubiquitous, for example, during metamorphism, metasomatism and weathering. These large–scale processes are often characterized by pseudomorphic mineral replacements as seen in albitisation, where Ca or K-rich feldspars are progressively replaced by the Na-rich plagioclase, albite (Hövelmann et al. 2010; Niedermeier et al. 2009; Engvik et al. 2011). During albitisation many elements are mobilized and removed into the fluid phase that may migrate through the rock and ultimately be associated with large-scale ore deposition. Replacement reactions also occur quite commonly in carbonate rocks, promoted by the higher solubility of carbonates compared to other rock-forming minerals. For example, calcite ($CaCO_3$) may be replaced by other carbonates such as dolomite or siderite (Pearce et al., 2013) or may form other calcium compounds when in contact with appropriate solutions. For example, calcite in contact with PO_4-bearing solutions is easily replaced by apatite, Ca-phosphate (Yoshimura et al. 2004; Kasioptas et al. 2011; Jonas et al. 2013, 2014; Pedrosa et al. 2016).

Replacement reactions are complex reactions controlled by at least three reaction steps: dissolution, mass transfer (including fluid migration through a porous solid phase and element diffusion through a fluid phase) and precipitation (including nucleation and growth). The kinetics of replacement reactions is dependent on the contribution of each of these steps and these may vary during the progression of the reaction. The overall reaction rate is generally dependent on the slowest of these reaction steps. The temperature dependence of the reaction rate is referred to

48 as the empirical activation energy (E_a), without specific reference to the overall rate-controlling
49 step.

50 A study by Xia et al. (2009) has shown that during mineral replacement reactions, when the rate-
51 controlling step is dissolution, there may be perfect preservation of the mineral microstructure
52 inherited from the parent phase (micro and nano-scale pseudomorphism). The relevance of
53 coupled dissolution-precipitation reactions to a wide range of fluid-solid reactions has been
54 recently reviewed by Ruiz-Agudo et al. (2014) and Altree-Williams et al. (2015). As well as
55 describing reequilibration reactions occurring in the Earth, these reactions may be used to design
56 new materials with specific engineered and functionalized properties. Examples of compositional
57 control and designed products include the use of apatite formed from the replacement of a
58 carbonate such as calcite or aragonite (Kasioptas et al. 2010). New bone replacement materials
59 (apatite) need to combine long implant life with compatibility and appropriate mechanical
60 properties and dissolution-precipitation is a process that has been proposed for the synthesis of
61 porous biocompatible material for bone implants (Heness and Ben-Nissan 2004).

62 In this paper we describe the replacement of calcite (Carrara marble) by fluorite (CaF_2).
63 Understanding the mechanism and kinetics of the replacement of carbonates by fluorite has
64 applications in both Earth sciences and engineering. Fluorite (CaF_2) occurs naturally in many
65 types of rocks (igneous, sedimentary, and metamorphic) and its origin is commonly associated
66 with hydrothermal fluids (e.g. Richardson and Holland 1979; Toft 1986; Gagnon 2003; Schwinn
67 and Markl 2005; Pradesh 2013). Fluorite pseudomorphs after calcite are not uncommon in nature
68 as evidenced in museum collections (e.g. from Chihuahua, Mexico). Fluorite is an important
69 industrial mineral. It is used in a wide variety of chemical, metallurgical and ceramic processes.
70 An environmentally important example is the mechanism of interaction of carbonates with

fluoride ions in drinking water. Fluoride has been added to town water supplies since the 1950s in Europe, the USA and Australia with the aim of reducing tooth decay. This replacement process results in a hardened surface of fluorapatite at the enamel (apatite) surface of the tooth (Pasteris and Ding 2009). According to the World Health Organization (WHO 2011), fluoride ingestion (through drinking water or a combination with other sources, such as fluoridated toothpaste) gives significant beneficial health effects at low concentrations, but at excessive exposure can result in adverse effects, such as dental and skeletal fluorosis. The WHO (2011) recommends a guideline of a maximum fluoride content of 1.5 mg/L for drinking water. Excessive fluoride exposure has been reported for many years and for a large number of developed and developing countries (Ghosh et al. 2013). This excess results from the accumulation of fluoride in groundwater (principal source of drinking water) from a number of different sources (e.g. fertilizer emission and mineral weathering) depending on the location (Brindha and Elango 2011). Calcite grains have been used as seed material in chemical reactors for the sequestration of fluoride from contaminated waters and wastewaters (Simonsson 1979; Yang et al. 1999; Turner et al. 2005; Aldaco et al. 2007), representing a direct application of the replacement of calcite by fluorite.

The aim of the present work is to investigate the kinetics of the replacement of calcium carbonate by fluorite as well as to understand better the mechanism of replacement reactions in general. Carrara marble was chosen as the parent material due to its high purity in calcium carbonate and its uniform grain-size allowing grain-boundary fluid migration to be observed within the experimental sample size. The kinetics of replacement was determined from the amount of fluorite formed as a function of temperature and reaction time, as determined from the Rietveld

93 analysis of X-ray powder diffraction (XRD) patterns. Morphological characteristics of the
94 product phase (studied by scanning electron microscopy, SEM) complement this study.

95 **Materials and Methods**

96 **Starting material**

97 Small cubes (3 × 3 × 3 mm) of Carrara marble (~ 99.7 wt% of $CaCO_3$ and ~ 0.3 wt% of Mg,
98 Pedrosa et al. 2016) were cut and reacted with a 4 *M* ammonium fluoride (NH_4F) solution (Alfa
99 Aesar GmbH 98.0 %). Given that the fluid capacity of the hydrothermal reactor was 2 mL, a
100 concentration of 4 *M* NH_4F was used to guarantee enough fluoride in solution to fully replace the
101 marble samples by fluorite. The initial pH of the solution was 7.5(2) and the initial weight of the
102 samples averaged 75(2) mg (standard deviation ± 3 %).

103 **Solubilities of calcite and fluorite at experimental conditions**

104 The solubilities of calcite and fluorite in water and at the experimental conditions were estimated
105 using the computer program PHREEQC (Parkhurst and Appelo 1999). The simulations were
106 made for an initial stage of the reaction using the same approach as in Pedrosa et al. (2016). In
107 pure water, with an increase of temperature (60 to 140 °C) the solubility of fluorite increases
108 whilst the solubility of calcite decreases (Table 1, log K). In 4 *M* NH_4F, given by the saturation
109 index (SI) fluorite is the least soluble phase for all experimental conditions (Table 1). The small
110 difference between the program estimation (Table 1) and the known empirical solubilities of
111 calcite and fluorite in pure water at STP (log K -8.47 and -10.46, respectively) supports the
112 reliability of the simulations.

113 **Hydrothermal experiments**

Hydrothermal experiments were performed at different reaction times and temperatures of 60, 80, 100, and 140 °C. Each marble cube was inserted into a Teflon®-lined reactor together with 2 mL of fluid. The Teflon® reactor was placed into a steel autoclave and tightly sealed to avoid any fluid loss during reaction. The pressure was autogenous. After reaction, the autoclaves were removed from the furnace and quickly cooled in a flow of compressed air to room temperature (~ 22 °C). The final pH values of the fluids were measured. The samples were washed with distilled water, left to dry overnight at 40 °C, weighed, and then powdered in an agate mortar. The reactions were repeated for reproducibility and similar results were obtained. The reproduced samples were used for imaging analysis. Calcium contents in the final fluids were measured using inductively-coupled plasma optical emission spectrometry (ICP-OES).

X-ray diffraction (XRD)

A X'Pert PW 3040 PANalytical diffractometer (CuKα1 radiation, step size = 0.014°, Johannson monochromator with a Ge crystal cut on plane (111)) and the X'Pert Data Collector software were used for the powder XRD measurements. The measurements were performed at room temperature in the range between $5° \leq 2\theta \leq 90°$. Each sample was measured for 128 min. The patterns were analysed qualitatively using PowderCell version 2.4 by comparing the measured peaks visually with the powder patterns for calcite (Maslen et al. 1993) and fluorite (Batchelder et al. 1964) from the Pearson's Crystal database. The fraction of fluorite present in each sample (α) was determined using Rietveld refinements performed with the EdPCR program of the FullProf Suite (version 2.05) and the above mentioned crystal structure data as starting structures.

Calculation of kinetic parameters using complementary methods

The kinetic description of the replacement reaction was made by determining the empirical activation energy (E_a), the pre-exponential factor (A), and the reaction model (more detailed description below). The kinetic parameters of the replacement of calcite by fluorite in a 4 *M* ammonium fluoride solution were empirically determined by the complementary use of model-fitting and model-free (isoconversional) methods described by Khawam and Flanagan (2005a). The model-free method permitted the calculation of E_a, and a statistical comparison with the E_a values obtained in the model-fitting method permitted the determination of the best fitting reaction model and a value of the pre-exponential factor A.

The main difference between these model-fitting and the model-free methods is that the first averages the activation energy over the whole reaction (i.e. it assumes that E_a does not change with time) and the second calculates the activation energy for different extents of reaction. Both methods are based on measuring the amount of fluorite formed as a function of time during isothermal runs at different temperatures (in this case 60, 80, 100, 140 °C). The model-free method allows the calculation of E_a independent of the choice of rate equation and is able to determine if the activation energy varies with the reaction progress (Khawam and Flanagan 2005a, 2005b; Hancock and Sharp 1972; Putnis 1992).

Model-fitting method. In this method the experimental data were fitted to a number of different rate equations (Table 2) to calculate the activation energy (E_a) of the reaction. The goodness of fit of the models was evaluated using the correlation coefficient (r). The mathematical basis of these models can be found in Khawam (2007). The general form of the rate equations is the integral rate law,

$$g(\alpha) = kt. \quad (1)$$

158 Where α is the fraction of fluorite formed, k (min^{-1}) is the rate constant, and t is the time in
159 minutes. The reaction rate constants (k) are obtained from the slope of the plot of g(α) against the
160 reaction time (t) from equation (1) for each of the four isothermal experiments (performed at 40,
161 60, 80, and 140 °C). E_a was calculated using each of the models listed in Table 2, from the slope
162 of the plot of ln k against $1/T$ from the natural logarithmic of the Arrhenius equation:

163 $$k = A\mathrm{e}^{\left(-\frac{Ea}{RT}\right)} \Leftrightarrow \ln k = \ln A - \left(\frac{Ea}{RT}\right). \quad (2)$$

164 Where A (min^{-1}) is the pre-exponential factor (also known as the frequency factor), R is the gas
165 constant (8.341 J/molK), and T is the temperature in K.

166 Additionally, from all fitted models there is one (model An, Table 2), that allows the calculation
167 of an n-value (or Avrami exponent) for each of the isothermal experiments. The value of n has
168 been used to infer a reaction mechanism for solid-state reactions from kinetic data (Hancock and
169 Sharp 1972) and has also been used to infer the mechanism of a replacement reaction (Kasioptas
170 et al. 2010, and references therein). It is calculated from the slope of the plot of – ln ln (1 - α)
171 against ln time (details of this method are given in Putnis 1992).

172 **Model-free (isoconversional) method.** In the model-free method E_a values are
173 calculated for different degrees of replacement. The time (t) needed for certain fractions of
174 fluorite to form (we chose $0.01 \leq \alpha \leq 0.99$, with steps of 0.01) were interpolated from the
175 experimental data. In the second step, the Arrhenius equation was substituted in eq. 1 giving,

176 $$\mathrm{g}(\alpha) = Ae^{\left(-\frac{Ea}{RT}\right)}t. \quad (3)$$

177 The natural logarithmic of eq. (3) gives eq. (4),

178 $$-\ln t = \ln\left(\frac{A}{g(\alpha)}\right) - \frac{Ea}{RT} \quad (4)$$

179 E_a values are obtained from the slope of the plot of –ln t as a function of 1/T (in 1/K). This
180 method does not allow the direct calculation of A (Khawam and Flanagan 2005a). A slightly
181 different formulation of equation 4 is given in Putnis (1992) where the determination of E_a,
182 independent of the choice of rate equation, is termed the "time to a given fraction" method.

183 **Scanning Electron Microscopy (SEM)**

184 For visualization of the replacement microstructures and reaction rims, two sample treatments
185 were made using the previously reacted cubes. A group of samples was sectioned through the
186 center, mounted in epoxy resin, and polished. Other samples were sectioned in different
187 directions and glued onto a glass slide (no polishing was made). All samples were C-coated for
188 imaging in a SEM (JEOL JSM-6610LV) equipped with energy-dispersive X-ray analysis (EDX),
189 and secondary and electron backscattered detectors.

190 **Results**

191 **X-ray diffraction (XRD) analysis**

192 XRD confirmed that the calcium carbonate rock samples were partially transformed into fluorite
193 during the reactions with ammonium fluoride (NH_4F) solutions. The peaks of all powder patterns
194 were identified as either calcite or fluorite. With increasing reaction times the intensity of the

calcite peaks decreased whilst the intensity of fluorite peaks increased (e.g. Fig. 1).

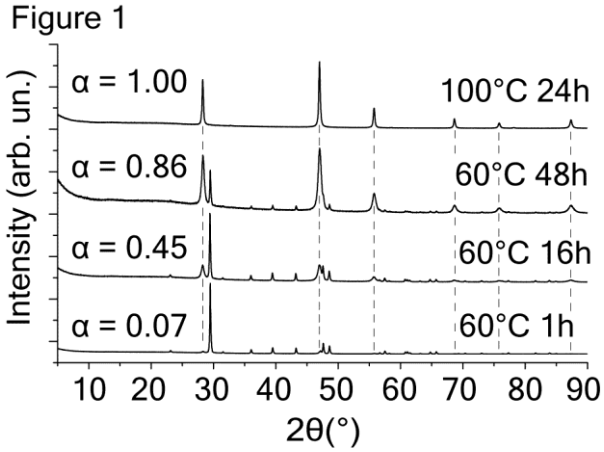

Figure 1. X-ray powder diffraction patterns showing the evolution of the parent and product phases from samples reacted at different reaction times and temperatures. The tracing indicates fluorite characteristic peak positions. The fraction of fluorite formed (α) was determined from Rietveld analysis.

The fractions of calcite and fluorite in each sample were obtained from Rietveld refinements (Table 3). The fractions of fluorite formed (α) are plotted against the reaction time for each of the isothermal experiments (Fig. 2).

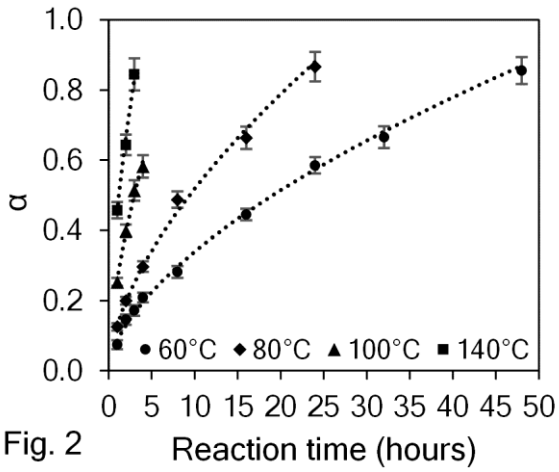

Fig. 2

206

207 **Figure 2.** Calculated fraction of fluorite formed (α), determined from the Rietveld refinements of
208 X-ray powder diffraction patterns of the mineral products resulting from the hydrothermal
209 experiments. The fitted lines are non-modelistic power law equations and were used for the
210 model-free (isoconversional) method.

211

212 **Kinetic analysis**

213 **Calculation of activation energy (model-fitting method).** With this method an
214 activation energy E_a was obtained from each model (Table 4). The E_a calculated with the
215 different models gave very similar results varying between 32 and 46 kJ/mol. Several models
216 had equivalent fitting coefficients (goodness of fit). If a most appropriate model was to be
217 selected using the goodness of fit, model D1 would be selected yielding an empirical activation
218 energy for the reaction of 41 kJ/mol.

219 From model An, ln-ln graphs were constructed for each of the isothermal experiments (Fig. 3).
220 The slopes of the graphs were 0.77, 0.82, 0.80 and 0.99 for the isothermal experiments
221 performed at 60, 80, 100 and 140 °C, respectively.

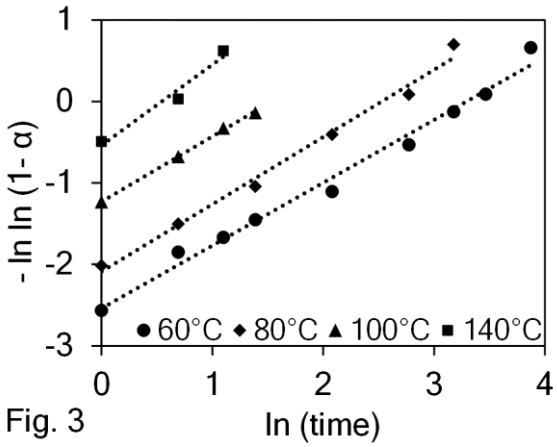

222

223 **Figure 3.** The plot of -ln ln (1-α) vs ln (time) for the replacement of calcite by fluorite that yield
224 n values of 0.77 (60°C), 0.82 (80°C), 0.80 (100°C) and 0.99 (140°C).

225

226 **Calculation of activation energy (model-free method).** With the model-free method the
227 E_a values were calculated for different fractions of replacement ($0.01 \leq \alpha \leq 0.99$). The
228 extrapolation of the time to the given fractions (α) was made using the trend-lines of the α – time
229 plots shown in Figure 2.

230 The E_a values (Fig. 4) vary between 39 and 49 kJ/mol, however 50 % of this variation occurs at
231 very low fractions of fluorite formed ($\alpha < 0.1$). This result is most probably an artifact and is
232 discussed later. For the fraction of fluorite formed between 0.10 and 0.99 E_a averaged 41(1)
233 kJ/mol.

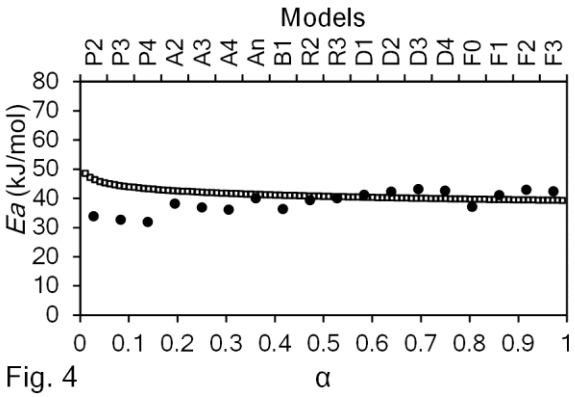

234 Fig. 4

235 **Figure 4.** Activation energies (E_a) for the replacement reaction calculated by: **(empty squares)**
236 the model-free method; **(circles)** the model-fitting method. Several E_a values of the model-fitting
237 method intersect the E_a values of the model-free method.

238

239 **Microstructural observations**

240 Hydrothermal treatment of the marble cubes produced perfect pseudomorphs, as measured from
241 the external dimensions of the reacted cubes. SEM analysis (Fig. 5a to 5e) shows the sharp
242 interface between the unreacted marble and the replacement product (fluorite). The replacement
243 reaction occurred homogeneously from the surface of the cubes into the center of the samples
244 (Fig. 5a to 5c). All samples showed very small amounts of fluorite precipitation adjacent to grain
245 boundaries ahead of the main reaction front (Fig. 5a to 5b). There is preservation of the grain
246 boundaries as can be seen in Fig. 5c. The marble and the fluorite have such similar morphologies
247 that they are almost indistinguishable at low magnification (Fig. 5d). At higher magnifications,
248 porosity of different sizes is seen in the fluorite rim (Fig. 5e). The pre-existent porosity present in
249 the marble (mostly grain boundaries) conferred a complex crystal microstructure to the newly
250 formed product phase (Fig. 5d, e, f). Overall the fluorite rim is composed of differently shaped
251 grains and the crystals of fluorite exhibit a needle-like morphology (Fig. 5e, f). Fluorite needles

do not seem to have any preferred orientation, with the exception of the reaction front, where they are mostly oriented perpendicular to it (Fig. 5f). Away from the reaction front, in many cases the fluorite crystals have healed (Fig. 5e), possibly related to the surface of the previous marble grains. This will be discussed more in the next section. A very small gap that is common to replacement reactions (Putnis 2009; Xia et al. 2009; Kasioptas et al. 2011) appears at the interface between the marble and fluorite (Fig. 5e) and has a variable size of 1.0(4) μm. There is a possibility that the gap could have formed or been widened during the quenching process. SEM-EDX analysis revealed that the low Mg content in the original marble (~ 0.3 wt%) was not included in the product phase (fluorite) crystal structure, but detected inside the pore spaces, where it probably precipitated (as any phase that includes Mg^{2+}, F^{-}, Na^{+}, and/or CO_3^{2-}) from remnant solution remaining in the pores after the reacted samples were cooled.

Figure 5

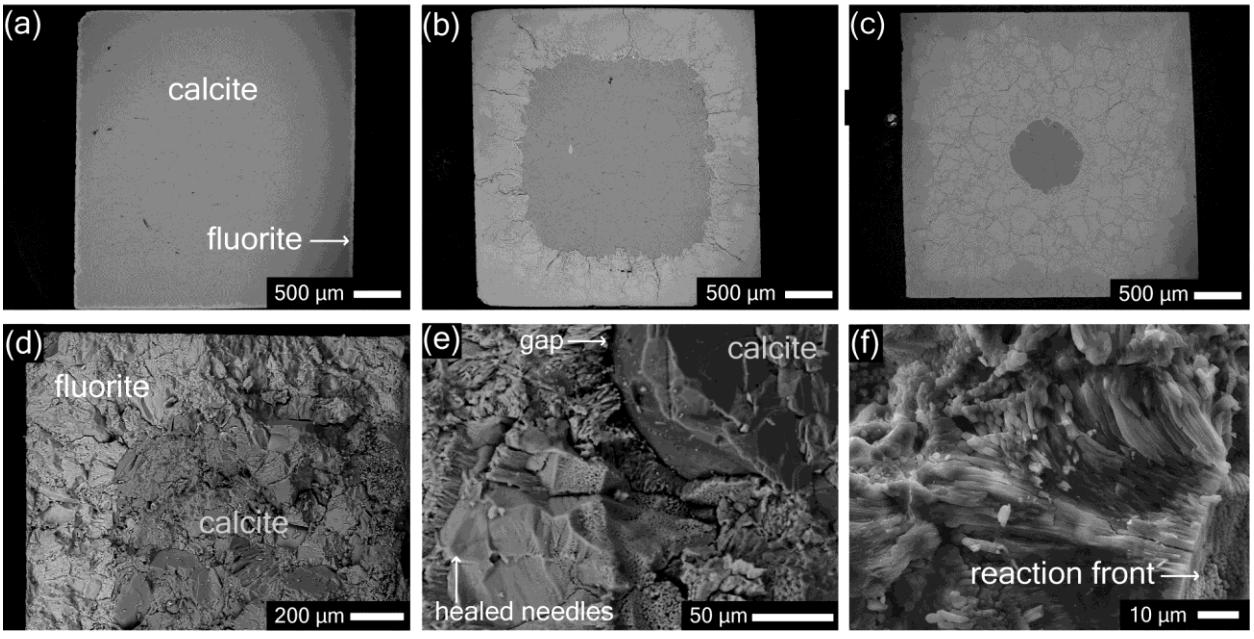

Figure 5. Images of cross-sections of cubes of Carrara marble reacted with a 4 M NH_4F solution: **a)** for 1 hour at 60 °C; **b)** for 48 hours at 60 °C; **c)** for 4 hours at 140 °C; **d)**, **e)**, and **f)** for 16 hours at 60 °C. All are BSE images with exception of f) that is SE.

Fluid changes after reaction

After all experiments, the pH of the fluids showed slight increases (Table 3). The increase of the pH was higher for higher reaction times. This is most probably related to the release of carbonates from the dissolution of calcite into the fluid phase. Calcium concentrations in the fluid after experiments were always lower than 0.5 ppm, corresponding to a maximum mass fraction Ca_{fluid}/Ca_{sample} of 0.0001.

The development of porosity

The development of porosity is an important characteristic of pseudomorphic replacement reactions (Putnis and Mezger 2004; Putnis et al. 2005). The amount of porosity formed in the samples can be calculated from the difference between the expected molar mass change if no porosity was formed and the actual mass change occurring in the samples. The calculated porosity (Table 3) correlates linearly (R^2= 98.9 %) with the fraction of fluorite formed measured with XRD. From this correlation (α [%] = 6.2736 × porosity [%] – 97.852) the calculated porosity for a fully reacted sample would be 31.5 %.

Discussion

In all hydrothermal experiments, known size cubes of Carrara marble (almost pure $CaCO_3$) were pseudomorphically replaced by fluorite (CaF_2). The degree of reaction was dependent on reaction time and temperature. The general equation that governs the replacement of calcite by fluorite can be written as, $CaCO_3$ (s) + 2 F^- (aq) ↔ CaF_2 (s) + CO_3^{2-} (aq).

Kinetic analysis

Activation energy from complementary methods. In this study we used the complementary method proposed by Kawam and Flanagan (2005b) to calculate the activation

289 energy of the replacement reaction. In this method, the most accurate activation energy is the one
290 calculated using the isoconversional (model-free) method and the best model should be the one
291 that results in an activation energy equal to the activation energy calculated with the model-free
292 method.

293 Activation energies calculated from the model-fitting method were very similar (32 to 46
294 kJ/mol). In this case, a statistical approach can be used (see next section) to select the best model
295 from the set of best models that resulted in the same E_a as in the model-free method (Khawam
296 and Flanagan 2005a). The model-free method resulted in an average activation energy of 41(1)
297 kJ/mol for fractions of fluorite (α) above 0.1. For $\alpha < 0.1$ the shape of the model-free
298 (isoconversional) plot (Fig. 4) is consistent with the shape of isoconversional plots of simulations
299 to which small time error shifts (minute-scale) were added (Kawam and Flanagan 2005b),
300 suggesting that the variation is an artifact, possibly caused by the experimental time being
301 controlled on an hour-scale.

302 **Selection of the best model.** Several models (An, R3, D1, and F1) resulted in an E_a
303 (Table 4) equal (41 ± 1 kJ/mol) to that calculated using the model-fitting method (Fig. 4). To
304 evaluate which is the most accurate of the five models, the fraction of fluorite formed (α) was
305 predicted with each of the four model equations. The model that results in the lowest standard
306 error of the estimate (σ_{est}) and lowest bias is considered the best model. Plots of model-predicted
307 versus experimental α values are shown in Fig. 6a to 6d. The model An (Table 2) resulted in the
308 lowest fit (R^2= 98.8 %), but had the lowest σ_{est} and the best accuracy (zero bias), therefore it
309 could have been considered the best model (Fig. 6a). However, the model contains a circular
310 argument because it includes n-values that were calculated from the experimental data (from the
311 slope of the graphs in Fig. 3), justifying its accuracy. The second best linear fit (R^2= 99.1 %) was

made using model R3 (Fig. 6b) but it had a σ_{est} of 0.08, and a negative bias of 50 %, which means this model could predict well between samples reacted for different reaction times, but the absolute values could be underestimated by an average of 50 %, making this the least appropriate model. The most accurate model is D1 with predictions that fitted the experimental data with R^2 of 99.6 %, a σ_{est} of 0.04 and a positive bias of 12 % (Fig. 6c). Model F1 (Fig. 6d) could not be considered the best model because it had a lower fit (98.5 %), a slightly lower σ_{est}, and a higher bias (34 %) than that of model D1. The diffusion model D1 is the model of choice for the replacement of Carrara marble by fluorite, yielding an activation energy of 41 kJ/mol, the same E_a calculated using the model-free method (for $\alpha > 0.1$), and an A of 732 min^{-1}, resulting in an integral rate law equation equal to $\alpha^2 = 732e^{(-41/RT)}t$.

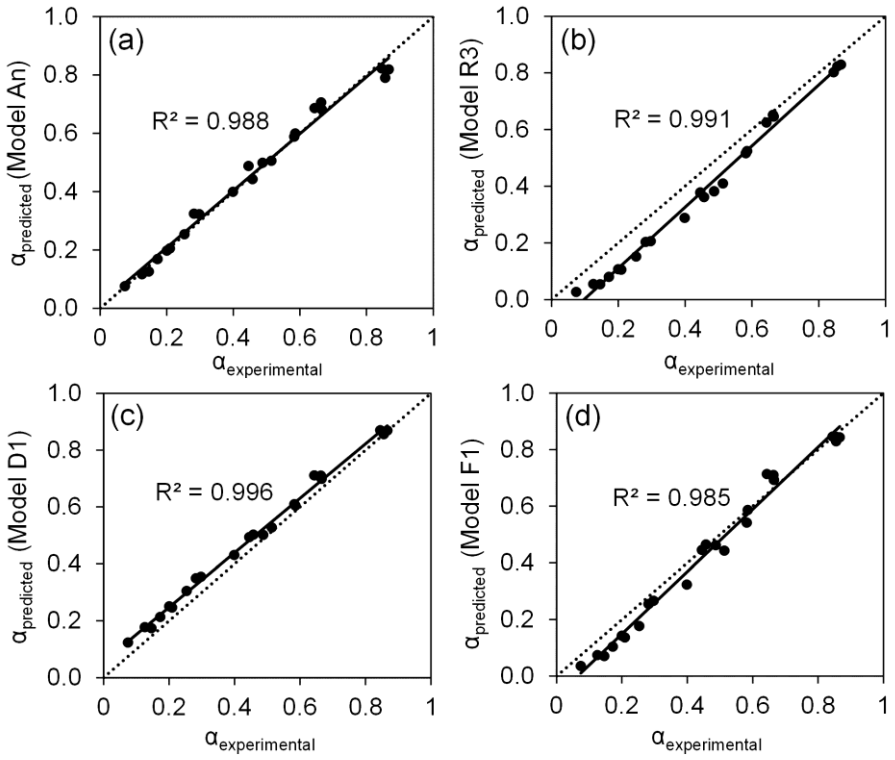

Figure 6. Model predicted ($\alpha_{predicted}$) against measured fractions of fluorite formed ($\alpha_{experimental}$) in the experiments: **a)** model An; **b)** model R3; **c)** model D1; **d)** model F1.

The Avrami exponential (n-value). If the mechanism of the reaction is the same for experiments at different temperatures, then they should be characterized by a constant n-value, and if the n-value changes then the rate-controlling kinetic mechanism could have changed (Avrami 1939). Results show very close n-values (0.77, 0.82, and 0.80) for the isothermal experiments carried out at 60, 80, and 100 °C, and these n-values stand between those that Hancock and Sharp (1972) interpreted as being diffusion and first-order kinetic controlled processes. For the 140 °C experiment the higher n-value (0.99) approximates mostly to a first-order kinetic controlled process (Hancock and Sharp 1972). Kasioptas et al. (2010) obtained similar n-values for the replacement of aragonite by apatite under mild hydrothermal conditions and interpreted the combination of these processes as being related to a control of the interfacial reaction. Results from Hancock and Sharp (1972) are based on kinetic studies of solid-state transformations and here we are investigating a fluid-mediated replacement reaction. Therefore we also interpret our results as interfacial reaction controlled, limited by the diffusion of ions through the fluid phase.

Experimental variation. For the determination of the reaction kinetics, potential experimental variables were held constant (as far as possible) so that any variation was solely due to the temperature change. In our study, the sources of experimental variation could have been due to the slight differences in the size of the samples (3 % variation) and their characteristic internal morphology, and variability in grain sizes (Carrara marble has grains of ~ 150 μm). The use of identical synthetic calcite samples could avoid such variations, however in this study we wanted to relate as much as possible to natural systems. The reactions were repeated for reproducibility and similar results were obtained.

Replacement reaction mechanism

Microscopic observations showing pseudomorphism, sharp interfaces between parent and product phases and the generation of porosity, all indicate that the replacement of the Carrara marble by fluorite occurs via an interface-coupled dissolution-precipitation process (Putnis 2009; Putnis and Putnis 2007). The replacement occurs by the coupling of dissolution and precipitation at the reaction interface resulting in the formation of porosity within the newly formed phase. As the reaction moves further into the parent phase, mass transport through the pores in the product becomes an increasingly important factor. Xia et al (2009) suggested that a sharp and narrow (micrometer scale) interface, between reacted and unreacted solids as observed here, suggests that the dissolution of the parent phase is the rate-determining step. However, a decrease in the rate of dissolution might as well be related to the time that ions take to travel through the pores to reach the reaction interface, creating the compositional conditions for further dissolution and precipitation (further discussion below).

The successful transformation of calcium carbonate by fluorite using NH_4F solutions has been reported before (Baer and Lewin 1970), and also using HF (Glover and Sippel 1962), NaF (Trautz and Zapanta 1961; Ames 1961), and NH_4HF_2 (Trautz and Zapanta 1961). The precipitation of fluorite at a mineral-fluid boundary layer, enriched in dissolved calcite ions, was also observed by Godinho et al. (2014). The replacement mechanism involves the dissolution of calcite and the precipitation of fluorite. In order to maintain external volume (pseudomorphic replacement), the rate of dissolution must equal the rate of precipitation and this can only be achieved when the reactions are coupled at the parent mineral-fluid interface. As soon as the calcite begins to dissolve in the presence of the F-bearing solution (undersaturated with respect to fluorite), Ca^{2+} ions are released to the solution at the mineral-fluid interface. Immediately this

boundary layer fluid becomes supersaturated with respect to the new phase, fluorite, which precipitates. The molar volume of fluorite (V_m= 24.5 cm^3/mol) is lower than that of calcite (V_m= 36.9 cm^3/mol). The result is a volume deficit reaction, shown in the high porosity in the fluorite product phase. The formation of an interconnected porosity (permeability) in the product phase enables the solution to penetrate the previously solid parent calcite and so the reaction is able to continue at a moving interface within the rock. The replacement of pure calcite by fluorite corresponds to a molar volume reduction of 33.5 %. This corresponds to the minimum porosity expected in a fully replaced sample of pure calcite. The porosity calculated here for a hypothetical fully reacted sample was slightly lower (31.5 %) but within estimation error. This might indicate that the fluorite density of these samples was slightly lower than that of pure crystalline fluorite, justifying its higher volume. The quantification of porosity will be the focus of a further study. Besides molar volume changes, solubility differences between parent and product phases can result in increased porosity in the product (Pollok et al. 2011). However, the calcium content measured in the fluids after replacement of the marble by fluorite (< 0.5 ppm), was not in a significant amount for mass balance equations.

The large relative change between each isothermal reaction plot (α vs reaction time, Fig. 2) reflects the high sensitivity of the replacement reaction to relatively narrow temperature increases (60, 80, 100, and 140 °C). Thus, temperature is a major driving force for the reaction and it correlates somewhat linearly to the replacement rates (Fig. 7).

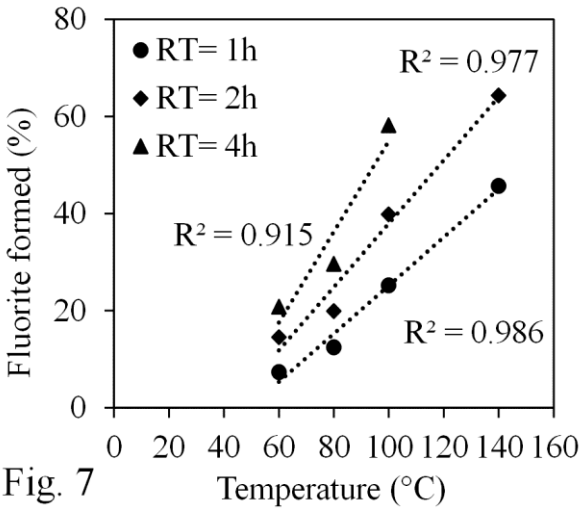

Fig. 7

Figure 7. Fluorite formed as a function of experimental temperatures for different reaction times. The amount of fluorite formed approximates to a linear relationship with the increase in temperature.

Backscatter SEM images showed that the evolution of the main reaction front (or bulk reaction) is very homogeneous (Fig. 5) forming an almost perfect sphere when it approaches the core of the sample. Fluid movement through grain boundaries can have a significant impact on replacement rates (Jonas et al. 2014), as grain boundaries are faster pathways for fast fluid transport. However, it has also been shown that fast reaction rates can result in replacements that proceed equally through grain boundaries and mineral grains (Pedrosa et al. 2016). In our experiments, replacement reactions were fast (especially at higher temperatures) and only small amounts of fluorite formed ahead of the reaction front next to grain boundaries and fractures, in agreement with Pedrosa et al. (2016).

406 The tight interface (~ 1 μm) between the parent and product phases shows that the degree of
407 coupling between the dissolution and precipitation is very high. From Xia et al. (2009) the
408 interpretation is that dissolution is the rate-controlling step. This results from the fact that if
409 dissolution is much faster than precipitation, the coupling between the two processes would be
410 lost, and thus, for a perfect pseudomorph to be formed, dissolution must be the rate-limiting step.
411 However if the rates of dissolution and precipitation are coupled and approximately equal, both
412 could be ultimately controlled by mass transport to and from the reaction interface. Dissolution
413 and precipitation rates are controlled by the saturation conditions of the interfacial fluid. It can be
414 assumed that the dissolution step is controlled by Ca^{2+} diffusion away from the dissolving calcite
415 surface and this can be caused by small concentration gradients at the narrow reaction front (~ 1
416 μm) caused by its consumption in the precipitation of fluorite (CaF_2). The precipitation of
417 fluorite is, in turn, controlled by the rate at which F^- arrives at the reaction interface, and may
418 control the overall reaction rate. The fact that a diffusion model best fitted the experimental data
419 from the calculated E_a suggests that it is effectively the overall mass transfer within the fluid
420 phase up to the reaction interface (as well as the reequilibration in the opposite direction in both
421 the fluid and solid phases) that dominates the replacement rate.

422 Results of the model-free method to calculate E_a suggest that the mechanism of replacement, and
423 hence the rate-controlling step did not change with the progress of reaction. Nevertheless, in all
424 isothermal experiments, the reaction rate slowed down with the progression of the reaction
425 (Table 3). This would be expected if the rate controlling step was diffusion, in which case the
426 rim thickness would vary as $t^{0.5}$ (Putnis and Mezger 2004). However, another possible cause of a
427 change in the kinetics could be due to morphology changes in the fluorite that affect the porosity.
428 Glover and Sippel (1962) showed that at the very early stages of replacement, the rate differs

429 from the rate after the reaction rim has formed and correlated it to the change in orientation of
430 the newly formed fluorite crystals. SEM images showed that the fluorite needle-like crystals are
431 oriented in many different directions, different from the reaction interface in which they are
432 oriented parallel, and also that the needles often have healed probably as the result of a
433 coarsening process. We hypothesize that this coarsening occurs at the outer edge of the replaced
434 grains, where the porosity is higher (more space for fluid passage) due to the presence of the
435 grain boundaries. This is consistent with textural equilibration where, as well as compositional
436 equilibration, simultaneously porosity begins to coarsen and then disappear in accordance with a
437 lowering of the energy state of the reaction product (Putnis et al. 2005). As soon as the outer
438 edge of the new fluorite grains is healed, no fluid can penetrate in that area leaving behind the
439 needle-like structure plus an impermeable outer surface, seen in Fig. 5e. The rim remained
440 permeable possibly because the grains did not heal completely. This process might have an
441 impact on the permeability of the rim, justifying the slower replacement rates for bigger
442 replacement rims.

443 Jonas et al. (2013) found that changes in the porosity during the replacement of calcite by apatite
444 resulted in kinetic data that could not be successfully fitted to Avrami rate equations. The smaller
445 difference in molar volumes, and hence porosity, and the higher reaction temperatures resulted in
446 more rapid textural equilibration in the reaction rims and hence greater variation in porosity. This
447 was reflected in changes in the rate controlling mechanism and hence activation energy during
448 the course of an isothermal reaction. In our case the consistent kinetics and the good fit between
449 the model-free and the model-dependent methods of determining activation energy suggest that
450 the overall mechanism of the replacement did not change as a function of temperature and time.

451 **Implications**

In this study we have determined the activation energy (E_a) for the replacement of calcite (as Carrara marble) by fluorite in F-rich solutions. By comparing different reaction models with the experimental kinetic data as a function of temperature, the best fit gave an activation energy, E_a value of 41 ± 1 kJ/mol. The discussion of the rate-determining step for a coupled dissolution-precipitation reaction has emphasized that dissolution, ion transport and precipitation cannot be simply separated as independent sequential processes in that both dissolution and precipitation depend on the fluid composition at the reaction interface. The conclusion that the overall replacement process is dependent on mass transport through the porous product phase (fluorite) is consistent with the determined value of E_a and the Avrami exponential n-value, and emphasizes the importance of the porosity generation in mineral replacement processes. The study provides data for future work on determining the mechanism of ion transport through micropores, notably the recent discussions on the role of charge gradients in small pores in enhancing transport by diffusioosmosis (Kar et al., 2016).

Environmental remediation is an important application of this replacement reaction. The study contributes to the understanding of the mechanism involved in the use of calcite source materials for the removal and/or recovery of fluoride from contaminated waters and wastewaters through the formation of a more stable phase (fluorite). A high calcite surface area and higher temperature will promote a faster replacement reaction and hence a more effective remediation of F-contaminated waters. Moreover, other cations in solution can be captured during this replacement due to the substitution for Ca^{2+} in the crystal structure of fluorite, such as the immobilization of radioactive strontium (Ames, 1960). This replacement can be used as a model system for understanding other geochemical reactions typically occurring in the Earth's crust, such as the partitioning of rare earth elements in fluorite (Schwinn and Markl, 2005). On the

other hand, the replacement of calcite by fluorite results in the release of carbonate into the fluid phase, affecting the local and/or global carbon cycle and therefore the redistribution of elements in the Earth's crust.

Acknowledgements

This project has received funding from the European Union's Seventh Framework Program for research, technological development and demonstration, a Marie Curie initial training network (Flowtrans) under grant agreement number 316889. Andrew Putnis and Christine V. Putnis also acknowledge funding within the EU Initial Training Networks CO2-React and MINSC.

References

Aldaco, R., Garea, A., and Irabien, A. (2007) Calcium fluoride recovery from fluoride wastewater in a fluidized bed reactor. Water Research, 41, 810–818.

Altree-Williams, A., Pring, A., Ngothai, Y., and Brugger, J. (2015) Textural and compositional complexities resulting from coupled dissolution–reprecipitation reactions in geomaterials. Earth-Science Reviews, 150, 628–651.

Ames, L.L. Jr. (1960) Anion replacement reactions for the removal of strontium from aqueous solutions, 34 p. Wash., U.S. Atomic Energy Commission.

Ames, L.L. Jr. (1961) The metasomatic replacement of limestones by alkaline, fluoride-bearing solutions. Economic Geology, 65, 730-739.

Avrami, M. (1939) Kinetics of phase change. I. General theory. The Journal of Chemical Physics, 7, 1103.

Baer, N.S., and Lewin, S.Z. (1970) The replacement of calcite by fluorite: A kinetic study. American Mineralogist, 55, 466-476.

497 Batchelder, D.N., and Simmons, R.O. (1964) Lattice constants and thermal expansivities of
498 silicon and of calcium fluoride between 6° and 322 °K. The Journal of Chemical Physics,
499 41, 2324-2329.
500 Brindha, K. and Elango, L. (2011) Fluoride in groundwater: causes, implications and mitigation
501 measures. In Monroy, S.D. (Ed.), Fluoride Properties, Applications and Environmental
502 Management, 111-136.
503 Engvik, A.K., Mezger, K., Wortelkamp, S., Bast, R., Corfu, F., Korneliussen, A., Ihlen, P.,
504 Bingen, B., and Austrheim, H. (2011) Metasomatism of gabbro - mineral replacement
505 and element mobilization during the Sveconorwegian metamorphic event. Journal of
506 Metamorphic Geology, 29, 399–423.
507 Gagnon, J.O.E.L.E. (2003) Compositional heterogeneity in fluorite and the genesis of fluorite
508 deposits: insights from LA – ICP – MS Analysis. The Canadian Mineralogist, 41, 365–
509 382.
510 Ghosh, A., Mukherjee, K., Ghosh, S. K., and Saha, B. (2013) Sources and toxicity of fluoride in
511 the environment. Research on Chemical Intermediates, 39, 2881-2915.
512 Glover, E.D., and Sippel, R.F. (1962) Experimental pseudomorphs: Replacement of calcite by
513 fluorite. American Mineralogist 47, 1156-1165.
514 Godinho, J.R.A., Putnis, C.V, and Piazolo, S. (2014) Direct observations of the dissolution of
515 fluorite surfaces with different orientations. Crystal Growth & Design, 29, 69-77.
516 Hancock, J., and Sharp, J. (1972) Method of comparing solid-state kinetic data and its
517 application to the decomposition of kaolinite, brucite, and $BaCO_3$. Journal of the
518 American Ceramic Society, 55, 74–77.
519 Heness, G., and Ben-Nissan, B. (2004) Innovative bioceramics. Materials Forum, 27, 104–114.

Hövelmann, J., Putnis, A., Geisler, T., Schmidt, B.C., and Golla-Schindler, U. (2010) The replacement of plagioclase feldspars by albite: Observations from hydrothermal experiments. Contributions to Mineralogy and Petrology, 159, 43–59.

Jonas, L., John, T., and Putnis, A. (2013). Influence of temperature and Cl on the hydrothermal re- placement of calcite by apatite and the development of porous microstructures: The American Mineralogist, 98, 1516–1525.

Jonas, L., John, T., King, H.E., Geisler, T., and Putnis, A. (2014) The role of grain boundaries and transient porosity in rocks as fluid pathways for reaction front propagation. Earth and Planetary Science Letters, 386, 64–74.

Kar, A., McEldrew, M., Stout, R.F., Mays, B.E., Khair, A., Velegol, D., and Gorski, C.A. (2016) Self-gnerated electrokinetic flows during pseudomorphic mineral replacement reactions. Langmuir, 32, 5233-5240.

Kasioptas, A., Geisler, T., Putnis, C.V, Perdikouri, C., and Putnis, A. (2010) Crystal growth of apatite by replacement of an aragonite precursor. Journal of Crystal Growth, 312, 2431–2440.

Kasioptas, A., Geisler, T., Perdikouri, C., Trepmann, C., Gussone, N., and Putnis, A. (2011) Polycrystalline apatite synthesized by hydrothermal replacement of calcium carbonates. Geochimica et Cosmochimica Acta, 75, 3486–3500.

Khawam, A., and Flanagan, D.R. (2005a) Complementary use of model-free and modelistic methods in the analysis of solid-state kinetics. Journal of Physical Chemistry B, 109, 10073–10080.

Khawam, A., and Flanagan, D.R. (2005b) Role of isoconversional methods in varying activation energies of solid-state kinetics: II. Nonisothermal kinetic studies. Thermochimica Acta, 436, 101–112.

Khawam, A. (2007) Application of solid-state kinetics to desolvation reactions, 321 p. Ph.D. thesis, University of Iowa.

Maslen, E.N., Streltsov, V.A., and Streltsova, N.R. (1993) X-ray study of the electron density in calcite, $CaCO_3$. Acta Crystallographica, Section B 49, 636-641.

Niedermeier, D.R.D., Putnis, A., Geisler, T., Golla-Schindler, U., and Putnis, C.V. (2009) The mechanism of cation and oxygen isotope exchange in alkali feldspars under hydrothermal conditions. Contributions to Mineralogy and Petrology, 157, 65–76.

Parkhurst, D.L., and Appelo, C.A.J. (1999) User's guide to PHREEQC (Version 2) - a computer program for speciation, batch-reaction, one-dimensional transport, and inverse geochemical calculations. U.S. Geological Survey, Water Resources, Denver, CO.

Pasteris, J.D., and Ding, D.Y. (2009) Experimental fluoridation of nanocrystalline apatite. American Mineralogist, 94, 53–63.

Pearce, M.A., Timms, N.E., Hough, R.M., and Cleverley, J.S. (2013) Reaction mechanism for the replacement of calcite by dolomite and siderite: Implications for geochemistry, microstructure and porosity evolution during hydrothermal mineralisation. Contributions to Mineralogy and Petrology, 166, 995–1009.

Pedrosa, E.T., Putnis, C.V., and Putnis, A. (2016) The pseudomorphic replacement of marble by apatite: The role of fluid composition. Chemical Geology, 425, 1–11.

562 Pollok, K., Putnis, C.V., and Putnis, A. (2011) Mineral replacement reactions in solid solution-
563 aqueous solution systems: Volume changes, reactions paths and end-points using the
564 example of model salt systems. American Journal of Science, 311, 211–236.
565 Pradesh, M. (2013) Occurrence of fluorine-bearing minerals in granite and a plausible mode of
566 transport of fluorine into hydrological system: an example from Jabalpur District, M.P.
567 India. Indian Journal of Geosciences, 66, 213-222.
568 Putnis, A. (1992) An Introduction to Mineral Sciences, 457 p. Cambridge University Press, U.K.
569 Putnis, A. (2002) Mineral replacement reactions: from macroscopic observations to microscopic
570 mechanisms. Mineralogical Magazine, 66, 689-708.
571 Putnis, A. (2009) Mineral replacement reactions. Reviews in Mineralogy and Geochemistry, 70,
572 87-124.
573 Putnis, A., and Putnis, C.V. (2007) The mechanism of reequilibration of solids in the presence of
574 a fluid phase. Journal of Solid State Chemistry 180, 1783-1786.
575 Putnis, C.V., and Mezger, K. (2004) A mechanism of mineral replacement: Isotope tracing in the
576 model system KCl-KBr-H_2O. Geochimica et Cosomochimica Acta, 68, 2039-2848.
577 Putnis, C.V., Tsukamoto, K., and Nishimura, Y. (2005) Direct observations of pseudomorphism:
578 compositional and textural evolution at a fluid-solid interface. American Mineralogist,
579 90, 1909-1912.
580 Richardson, C.K., and Holland, H.D. (1979) Fluorite deposition in hydrothermal systems.
581 Geochimica et Cosmochimica Acta, 43, 1327–1335.
582 Ruiz-Agudo, E., Putnis, C.V., and Putnis, A. (2014) Coupled dissolution and precipitation at
583 mineral–fluid interfaces. Chemical Geology, 383, 132–146.

584 Schwinn, G., and Markl, G. (2005) REE systematics in hydrothermal fluorite. Chemical
585 Geology, 216, 225–248.
586 Simonsson, D. (1979) Reduction of fluoride by reaction with limestone particles in a fixed bed.
587 Industrial & Engineering Chemistry Process Design and Development, 18, 288-292.
588 Toft, P.C. (1986) Diagenetic fluorite in chalks from Stevns Klint and Møns Klint, Denmark.
589 Sedimentary Geology, 46, 311–323.
590 Trautz, O.R., and Zapanta R.R. (1961) Experiments with calcium carbonate phosphates and the
591 effect of topical application of sodium fluoride. Archives of Oral Biology, 4, 122-133.
592 Turner, B.D., Binning, P., and Stipp, S.L.S. (2005) Fluoride removal by calcite: Evidence for
593 fluorite precipitation and surface adsorption. Environmental Science and Technology, 39,
594 9561–9568.
595 WHO (2011) Guidelines for drinking-water quality. World Health Organization (WHO) Geneva.
596 Xia, F., Chen, G., Ngothai, Y., O'Neill, B., Putnis, A., and Pring, A. (2009) Mechanism and
597 kinetics of pseudomorphic mineral replacement reactions: a case study of the replacement
598 of pentlandite by violarite. Geochimica et Cosmochimica Acta ,73, 1945–1969
599 Yang, M., Hashimoto, T., Hoshi, N., and Myoga, H. (1999) Fluoride removal in a fixed bed
600 packed with granular calcite. Water Research, 33, 3395–3402.
601 Yoshimura, M., Sujaridworakun, P., Koh, F., Fujiwara, T., Pongkao, D., and Ahniyaz, A. (2004)
602 Hydrothermal conversion of calcite crystals to hydroxyapatite. Materials Science and
603 Engineering C, 24, 521–525.
604
605
606

607 **Tables**

608 **Table 1**. The solubility of calcite and fluorite in water and their saturation indices (SI) in 4 *M*
609 NH_4F at 25 °C and at experimental temperatures (PHREEQC calculations).

	Pure water		**4 *M* NH_4F**	
***T* (°C)**	**Calcite (log K)**	**Fluorite (log K)**	**Calcite (SI)**	**Fluorite (SI)**
25	-8.5	-10.6	0.8	9.8
60	-8.8	-10.3	0.0	9.4
80	-9.0	-10.2	-0.5	9.2
100	-9.3	-10.2	-0.9	9.1
140	-10.0	-10.2	-1.4	8.9

610

611 **Table 2.** Reaction models employed to fit the empirical data (adapted from Khawam and
612 Flanagan, 2005b).

Model	**Integral Rate law $g(\alpha) = kt$**
Nucleation and Growth	
Power-law (P2)	$\alpha^{\left(\frac{1}{2}\right)}$
Power-law (P3)	$\alpha^{\left(\frac{1}{3}\right)}$
Power-law (P4)	$\alpha^{\left(\frac{1}{4}\right)}$

Avrami Erofeev (A2)	$\left[-\ln(1-\alpha)\right]^{\frac{1}{2}}$
Avrami Erofeev (A3)	$\left[-\ln(1-\alpha)\right]^{\frac{1}{3}}$
Avrami Erofeev (A4)	$\left[-\ln(1-\alpha)\right]^{\frac{1}{4}}$
Avrami Erofeev (An)	$\left[-\ln(1-\alpha)\right]^{\frac{1}{n}}$
Prout–Tompkins (B1)	$\ln\left[\frac{\alpha}{1-\alpha}\right]$
Geometrical contraction	
Contracting area (cylinder) (R2)	$[1-(1-\alpha)^{1/2}]$
Contracting volume (sphere) (R3)	$[1-(1-\alpha)^{1/3}]$
Diffusion	
1-D diffusion (D1)	α^2
2-D diffusion (D2)	$\left[(1-\alpha)\ln(1-\alpha)\right]+\alpha$
3-D diffusion (D3)	$\left[1-(1-\alpha)^{\frac{1}{3}}\right]^2$
Ginstling–Brounshtein (D4)	$1-\left(\frac{2\alpha}{3}\right)-(1-\alpha)^{2/3}$
Reaction-order	

Zero-order (F0)	α
First-order (F1)	$-\ln(1-\alpha)$
Second-order (F2)	$(1-\alpha)^{-1}-1$
Third-order (F3)	$0.5\left((1-\alpha)^{-2}-1\right)$

613

614 **Table 3.** Results of the hydrothermal experiments including, the initial mass of the samples, its
615 mass change (%) after reaction, the porosity (%) calculated from the expected against actual
616 mass change, the percentage of fluorite in each sample, and the overall rate at which fluorite
617 formed in each experiment.

T **(°C)**	**Reaction time (h)**	$m_{initial}$ **(mg)**	$m_{decrease}$ **(%)**	pH_{final}	**Porosity (%)**	CaF_2 **(%)**	**Reaction rate** (mg_{CaF2}/h)
60	1	76	1.7	8.1	16.2	7	7
60	2	76	3.3	8.2	17.6	15	7
60	3	73	4.0	8.3	18.2	17	6
60	4	73	5.1	8.3	19.1	21	5
60	8	73	6.3	8.4	20.1	28	4
60	16	76	9.3	8.6	22.7	45	3
60	24	76	11.7	8.7	24.7	59	2
60	32	76	13.2	8.7	26.0	67	2
60	48	76	15.9	8.8	28.3	86	2

80	1	76	2.9	8.1	17.2	13	13
80	2	76	5.2	8.4	19.2	20	10
80	4	76	6.7	8.5	20.5	30	7
80	8	71	10.4	8.6	23.7	49	6
80	16	76	13.4	8.7	26.2	66	4
80	24	76	16.3	8.8	28.7	87	4
100	1	76	5.5	8.4	19.5	25	25
100	2	76	9.0	8.5	22.4	40	20
100	3	73	11.0	8.6	24.2	51	17
100	4	68	12.6	8.6	25.5	58	15
140	1	74	10.0	8.5	23.3	46	46
140	2	75	13.7	8.7	26.4	64	32
140	3	76	16.6	8.8	29.0	84	28

Table 4. Calculated kinetic parameters (pre-exponential factor, A, and activation energy, E_a) using the model-fitting method for the isothermal experiments performed in this study.

Model	A **(min^{-1})**	E_a **(kJ/mol)**	r^a
P2	4.88×10^1	34	0.9721
P3	2.46×10^1	33	0.9637
P4	1.58×10^1	32	0.9590
A2	3.65×10^2	38	0.9911[b]

A3	1.67×10^2	37	0.9860
A4	1.01×10^2	36	0.9824
An[d]	7.29×10^4	40	0.9925[b]
B1	6.88×10^2	36	0.9814
R2	2.99×10^2	39	0.9952[b]
R3[d]	2.86×10^2	40	0.9949
D1[c,d]	7.32×10^2	41	0.9968[b]
D2	8.06×10^2	42	0.9897
D3	3.96×10^2	43	0.9732
D4	2.38×10^2	43	0.9848
F0	1.88×10^2	37	0.9895
F1[d]	1.69×10^3	41	0.9906[b]
F2	8.60×10^3	43	0.9530
F3	2.37×10^4	42	0.9073

a) Correlation coefficient g(α) vs *t* (min).

b) Equivalent models based on goodness of fit.

c) Model selected based on model-fitting method.

d) Models that E_a resulted to be equal to the E_a calculated with the model-free method (41(1) kJ/mol).